Biomimetic design of microfluidic manifolds based on a generalised Murray's law†

David R. Emerson,[a] Krzysztof Cieślicki,[b] Xiaojun Gu[a] and Robert W. Barber[a]

Received 30th November 2005, Accepted 24th January 2006
First published as an Advance Article on the web 9th February 2006
DOI: 10.1039/b516975e

The relationship governing the optimum ratio between the diameters of the parent and daughter branches in vascular systems was first discovered by Murray using the principle of minimum work. This relationship is now known as Murray's law and states that the cube of the diameter of the parent vessel must equal the sum of the cubes of the daughter vessels. For symmetric bifurcations, an important consequence of this geometric rule is that the tangential shear stress at the wall remains constant throughout the vascular network. In the present paper, we extend this important hydrodynamic concept to arbitrary cross-sections and provide a framework for constructing a simple but elegant biomimetic design rule for hierarchical microfluidic networks. The paper focuses specifically on constant-depth rectangular and trapezoidal channels often employed in lab-on-a-chip systems. To validate our biomimetic design rule and demonstrate the application of Murray's law to microfluidic manifolds, a comprehensive series of computational fluid dynamics simulations have been performed. The numerical predictions are shown to be in very good agreement with the theoretical analysis, confirming that the generalised version of Murray's law can be successfully applied to the design of constant-depth microfluidic devices.

1 Introduction

Nature has perfected many techniques and solutions that surpass man-made designs. However, recent technological advances have brought a greater understanding of fundamental properties and processes and it has become possible to attempt to 'mimic' or synthesize what nature does naturally. This field, now known as *biomimetics*, covers many new and emerging topics and offers significant potential in the further development of MEMS,[1] microfluidic devices,[2,3] and lab-on-a-chip systems.[4] Biomimetic designs can encompass surface treatments that mimic physiological processes or use biological principles to enhance performance through geometric optimisation.

One example that could play a significant role in improved flow control through microfluidic devices is mimicking the structure of vascular trees. Biological systems of blood vessels are usually arranged in hierarchical structures and a distinctive feature of this arrangement is their multi-stage division or bifurcation. At each generation, the characteristic dimension of the vascular segments will generally become smaller, both in length and diameter. Similar configurations occur in microfluidic manifolds with the inlet channel branching into smaller channels[5] as illustrated schematically in Fig. 1.

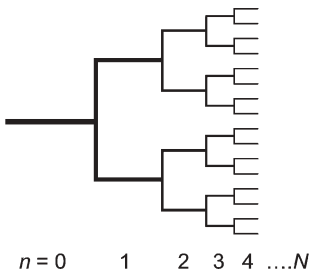

Fig. 1 Schematic diagram of a bifurcating vascular network.

In contrast to biological vascular networks, which are composed of circular pipes, microfluidic manifolds are fabricated from a range of processes that include photolithography, wet or dry etching, and surface micromachining. The various approaches can result in channels with very characteristic geometric shapes *e.g.* wet etching a <100> silicon wafer with KOH gives a trapezoidal section with an angle of 54.74°. A common feature in fabricating these channels is that the depth remains constant throughout the device.

A method of fabricating multi-depth microfluidic manifolds has recently been described by Lim *et al.*[6] who used a maskless direct-write method with a Nd:Yag laser to create the multi-level channels. One of their designs was based upon biomimetic principles but it was restricted to channels with a square cross-section. Their study compared the performance of a conventional constant-depth (non-biomimetic) manifold with that of a multi-depth artificial vasculature and they clearly demonstrated the potential benefits of employing a biomimetic design. Although Lim *et al.*'s novel fabrication approach allows multi-depth channels to be manufactured, to date, no theory has been available to support the design of

[a]*Centre for Microfluidics and Microsystems Modelling, CCLRC Daresbury Laboratory, Daresbury, Warrington, WA4 4AD, England*
[b]*Institute of Automatic Control and Robotics, Warsaw University of Technology, św. A. Boboli 8, 02-525 Warsaw, Poland*

† Electronic supplementary information (ESI) available: Colour contour plots of computed velocity distribution at the first T-junction and 90° bend for an inlet Reynolds number of 250. See DOI: 10.1039/b516975e

constant-depth micro-channels that obey biomimetic principles. If lab-on-a-chip systems are to benefit from a biomimetic approach, the design rules need to comply with more conventional fabrication practices (*e.g.* standard photolithography, LIGA) and not introduce additional complexity through numerous alignment steps and multiple exposure stages associated with multi-level microstructures.

In this paper, a tree-like model of micro-channels is proposed that mimics the geometrical properties of vascular systems. The paper provides a theoretical basis for understanding flow behaviour in fluidic networks that obey vascular principles and demonstrates how flow properties can be controlled within symmetric tree-like structures composed of either square, rectangular or trapezoidal micro-channels. To support the theoretical analysis, a detailed numerical modelling study is presented that demonstrates how the theory can be used to understand, predict and control the flow through branching micro-channel networks.

2 Theoretical background

Branching structures found in mammalian circulatory and respiratory systems have, through natural selection, evolved over many millennia to their current state of minimising the amount of biological work required to operate and maintain the system. A relationship between the diameter of the parent branching vessel and the optimum diameters of the daughter vessels was first derived by Murray[7] using the principle of minimum work. This relationship is now known as *Murray's law* and states that the *cube* of the diameter of a parent vessel (d_0) equals the sum of the cubes of the diameters of the daughter vessels *i.e.* $d_0^3 = d_1^3 + d_2^3$. Regrettably, the work of Murray was overlooked for almost 50 years[8] but vascular trees and scaling laws are now receiving much attention, particularly in the biological world.[9–15] However, with the exception of the brief study by Lim *et al.*,[6] there appears to be little application of Murray's law to the design of man-made structures and, in particular, to the geometric design of microfluidic channels and manifolds.

For a symmetric bifurcation where $d_1 = d_2$, it follows that

$$d_0^3 = 2d_1^3 \tag{1}$$

Using eqn (1), it is possible to obtain relationships between vessel diameters, average velocity, wall shear stress, flow resistance, and pressure for each consecutive generation. It has also been shown[16] that Murray's law can be generalised if the change in diameter of each consecutive generation can be represented by a *branching parameter*, X:

$$X = \frac{d_0^3}{2d_1^3} \tag{2}$$

For $X = 1$, the parent/daughter branches obey Murray's original hypothesis. However, X does not have to be unity, although the resulting system will no longer obey the minimum work principle. As will be described later, the generalised case of $X \neq 1$ can be used to design microfluidic manifolds with specific properties. If the value of the parameter X is held constant throughout the branching hierarchy, the segment diameter of the nth generation is given by

$$d_n = \frac{d_0}{(2X)^{n/3}} \tag{3}$$

For a symmetric system, the volumetric flow rate halves at each bifurcation *i.e.* $Q_n = 2^{-n} Q_0$, and therefore, using eqn (3), the mean flow velocity, V_n, in each generation can be shown to be

$$V_n = \frac{Q_n}{A_n} = V_0 \left(\frac{X^2}{2}\right)^{n/3} \tag{4}$$

where A_n is the cross-sectional area of the nth generation. The tangential shear stress acting on the wall of a circular pipe in a fully-developed laminar flow can be written as[17]

$$\tau = \frac{8\mu V}{d} \tag{5}$$

where μ is the viscosity. Substituting eqn (3) and (4) into (5) gives an important relationship

$$\tau_n = \tau_0 X^n \tag{6}$$

where τ_0 is the tangential wall shear stress in the entrance channel ($n = 0$). By changing the value of the branching parameter, X, it is possible to introduce an element of control into the flow behaviour.

2.1 Application of Murray's law to rectangular and square cross-sections

Murray's law was originally derived for biological systems where the 'channels' all have a circular cross-section. However, it is possible to extend this law to other geometries since there will be a direct analogy with the hydraulic diameter of the respective cross-sections. For a circular pipe, the stress distribution around the circumference will be uniform. In contrast, the wall shear stress in a non-circular channel will vary around the wetted perimeter. This difference can be taken into account by considering the *average* shear stress around the perimeter of the channel. The mean tangential wall shear stress, $\bar{\tau}$, can be related to the Fanning friction factor,[18] f, as follows

$$\bar{\tau} = \frac{1}{2}\rho V^2 f = \frac{1}{2}\rho V^2 \,\mathrm{Po}/\mathrm{Re} = \mu V \,\mathrm{Po}/(2D_\mathrm{h}) \tag{7}$$

where $\mathrm{Po} = f\,\mathrm{Re}$ is the Poiseuille number, $D_\mathrm{h} = 4 \times$ area/perimeter is the hydraulic diameter, and Re is the Reynolds number based on the mean velocity and hydraulic diameter.

Murray's original hypothesis leads directly to eqn (6) and, by analogy, we therefore propose the following biomimetic principle for the design of non-circular cross-sections:

$$\bar{\tau}_n = \bar{\tau}_0 X^n \tag{8}$$

The principle of using a specific shear stress distribution throughout the network provides a design rule that offers the potential to control the flow within a network of branching channels. It is also possible to use other flow properties (*e.g.*

mean velocity, Reynolds number) as the basis for the design methodology. However, only the shear stress analogy proposed in eqn (8) is based on a true biomimetic principle. Using eqn (8), it follows that

$$V_n \mathrm{Po}_n / D_{\mathrm{h}n} = V_0 \mathrm{Po}_0 X^n / D_{\mathrm{h}0} \tag{9}$$

The relationship given by eqn (9) must hold *regardless* of the shape of the channel but requires a knowledge of the hydraulic diameter and the Poiseuille number.

Fig. 2 shows the geometric properties of the two channels under investigation. For the rectangular channel, we define the aspect ratio of the nth generation as $\alpha_n = d/w_n$. At each bifurcation, the volumetric flow rate will halve and the relationship between the mean velocities is

$$V_n / V_0 = 2^{-n} A_0 / A_n \tag{10}$$

For constant-depth rectangular channels, the area and hydraulic diameter ratios can be written as

$$A_n / A_0 = \alpha_0 / \alpha_n \text{ and } D_{\mathrm{h}n} / D_{\mathrm{h}0} = (1 + \alpha_0)/(1 + \alpha_{\mathrm{n}}) \tag{11}$$

The Poiseuille number for fully-developed laminar flow through a rectangular channel can be obtained from the polynomial expression derived by Shah and London:[18]

$$\mathrm{Po}(\alpha_n^*) = 24[1 - a_1\alpha_n^* + a_2(\alpha_n^*)^2 - a_3(\alpha_n^*)^3 + a_4(\alpha_n^*)^4 - a_5(\alpha_n^*)^5] \tag{12}$$

where the required coefficients are $a_1 = 1.3553$, $a_2 = 1.9467$, $a_3 = 1.7012$, $a_4 = 0.9564$ and $a_5 = 0.2537$, respectively. However, for this particular problem an analytical solution exists and is given by

$$\mathrm{Po}(\alpha_n^*) = \frac{24}{\left[1 - \frac{192}{\pi^5}\frac{1}{\alpha_n^*}\sum_{i=1,3,5\ldots}^{\infty}\frac{1}{i^5}\tanh\left(\frac{i\pi\alpha_n^*}{2}\right)\right]\left(1+\frac{1}{\alpha_n^*}\right)^2} \tag{13}$$

Equations (12) and (13) require that $\alpha_n^* \leqslant 1$ which implies that $w_n \geqslant d$. To obtain the Poiseuille number when the width is less than the depth ($\alpha_n > 1$), it is necessary to set $\alpha_n^* = w_n/d$ but it is important to note that α_n remains as previously defined, *i.e.* $\alpha_n = d/w_n$. Substituting eqn (10) and (11) into (9) shows that the biomimetic design can be obtained by solving the following relationship:

$$\alpha_n(1 + \alpha_{\mathrm{n}})\,\mathrm{Po}(\alpha_n^*) = (2X)^n\,\alpha_0\,(1 + \alpha_0)\,\mathrm{Po}(\alpha_0^*) \tag{14}$$

Any appropriate method for finding the root, $\alpha_n = d/w_n$, can be used but as the function is well behaved, a simple bisection method, based on the approach described by Press *et al.*,[19] was employed in the present study. It should be noted that the solution specified by eqn (14) can be 'inverted' *i.e.* if the design engineer knows the dimensions of the smallest channel (corresponding to α_n) then the dimensions of the inlet channel and all other channels can be found.

For a manifold consisting of square channels, where the depth will change at each bifurcation, the area ratio and the hydraulic diameter ratio reduce to

$$A_n / A_0 = d_n^2 / d_0^2 \text{ and } D_{\mathrm{h}n} / D_{\mathrm{h}0} = d_{\mathrm{n}} / d_0 \tag{15}$$

The analysis of square channels is further simplified because the Poiseuille number will be identical at each successive generation and eqn (9) reduces to eqn (3) which can be solved analytically.

2.2 Application of Murray's law to trapezoidal silicon micro-channels

To simplify the analysis of <100> silicon trapezoidal sections, we define the aspect ratio as $\gamma = d/a$ (see Fig. 2) and note that the cross-sectional area and hydraulic diameter can be written as $(\sqrt{2}-\gamma)d^2/\sqrt{2}\gamma$ and $2d(\sqrt{2}-\gamma)/(\sqrt{2}+\gamma(\sqrt{3}-1))$, respectively. After some mathematical manipulation, it can be shown that we need to solve:

$$\frac{\sqrt{2}\gamma_n + (\sqrt{3}-1)\gamma_n^2}{(\sqrt{2}-\gamma_n)^2}\mathrm{Po}(\gamma_n) = (2X)^n \frac{\sqrt{2}\gamma_0 + (\sqrt{3}-1)\gamma_0^2}{(\sqrt{2}-\gamma_0)^2}\mathrm{Po}(\gamma_0) \tag{16}$$

For many practical channel shapes, including trapezoidal channels, the Poiseuille number cannot be obtained analytically. However, Morini[20] has shown that the Poiseuille number for KOH-etched silicon channels can be obtained from a 5th order polynomial as follows

$$\mathrm{Po}(\gamma_n) = 24\,[1 - b_1\gamma_n + b_2\gamma_n^2 - b_3\gamma_n^3 + b_4\gamma_n^4 - b_5\gamma_n^5] \tag{17}$$

where the coefficients have the values of $b_1 = 1.7611$, $b_2 = 2.6780$, $b_3 = 4.9342$, $b_4 = 10.0883$ and $b_5 = 7.4496$, respectively. The maximum value of the aspect ratio, γ, is limited to $1/\sqrt{2}$ (corresponding to $b = 0$ in Fig. 2) and, in practice, it is easier to solve eqn (16) using a change of variable with $\beta = d/b$ and setting $\gamma = \beta/(1+\sqrt{2}\beta)$. In this case, the parameter range for the aspect ratio is $0 \leqslant \beta \leqslant \infty$. For a manifold consisting of KOH-etched triangular channels or grooves (*i.e.* $b = 0$), where the width and

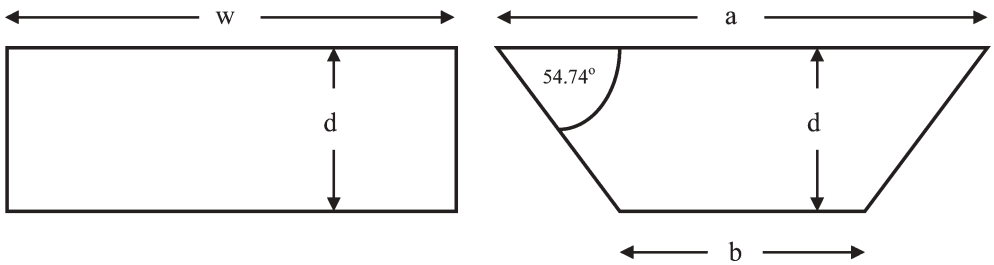

Fig. 2 Schematic representation of rectangular and trapezoidal <100> silicon micro-channel geometries.

depth will change at each bifurcation, the area ratio and the hydraulic diameter ratio again reduce to eqn (15). As in the case of the square channel, the Poiseuille number is constant at each bifurcation level and eqn (9) again reduces to eqn (3) allowing the problem to be solved analytically for either the width or the depth.

2.3 Total flow resistance and pressure distribution

An important issue in the design of any microfluidic manifold is the estimation of the total flow resistance and the pressure distribution within the network. The hydraulic resistance of a channel is defined as $\Delta P/Q$, and can be obtained by equating the pressure drop, ΔP, and shear forces acting on the fluid. It can be shown that the hydraulic resistance, R, of a single segment can be written as

$$R = \frac{\mu \mathrm{Po}\, 2L}{A\, D_{\mathrm{h}}^2} \tag{18}$$

where L is the length of the channel. In biological systems, the length of an individual segment is often proportional to its diameter.[21] To extend Murray's law to non-circular micro-channels, we have generalised this biological principle and have assumed that the length of each segment is proportional to its *hydraulic diameter*, D_{h}. The resistance of a single segment in the nth generation can therefore be written as

$$R_n \propto \frac{\mathrm{Po}_n}{A_n\, D_{\mathrm{h}n}} \tag{19}$$

Using eqn (9), (10) and (19) allows the hydraulic resistance of the individual segments to be related to the branching parameter, X:

$$\frac{R_n}{R_0} = (2X)^n \tag{20}$$

The total resistance of the manifold, R_{T}, can then be obtained using the analogy between pipe friction and electrical resistance. Using the fact that the individual segments within a given generation are in parallel gives:

$$R_{\mathrm{T}} = R_0 + \frac{R_1}{2} + \frac{R_2}{4} + \frac{R_3}{8} + \ldots + \frac{R_n}{2^n} + \ldots + \frac{R_N}{2^N} \tag{21}$$

and the total resistance of a manifold with N bifurcation levels will therefore be

$$R_{\mathrm{T}} = R_0 \sum_{i=0}^{N} X^i = R_0 \frac{X^{N+1} - 1}{X - 1} \tag{22}$$

The analogy between pipe friction and electrical resistance also allows the pressure distribution to be determined throughout the network. If the pressure at the inlet of the manifold is p_{in} and the pressure at the outlet is p_{out}, then it can be shown that the relative pressure at the entrance to the nth generation can be written as

$$\frac{p_n - p_{\mathrm{out}}}{p_{\mathrm{in}} - p_{\mathrm{out}}} = \frac{\sum_{i=n}^{N} X^i}{\sum_{i=0}^{N} X^i} = \left(\frac{X^{N+1} - X^n}{X^{N+1} - 1} \right) \tag{23}$$

The relationships given in eqn (22) and (23) hold regardless of the cross-sectional geometry, although it should be realised that each segment must adhere to the biomimetic principle that its length is proportional to its hydraulic diameter. However, it is not an essential requirement for the channel length to be proportional to the hydraulic diameter to exploit biomimetic design principles but the flow resistance and pressure distribution will no longer obey eqn (22) and (23).

3 Numerical simulation of micro-channels designed using Murray's law

To validate the theory outlined in Section 2 and demonstrate how Murray's law can be applied to the design of microfluidic manifolds, a comprehensive series of computational fluid dynamics (CFD) simulations have been performed. The simulations considered branching networks composed of square, rectangular, and trapezoidal cross-sections. The channel dimensions within each of the hierarchical networks are presented in Tables 1 and 2 while Fig. 3 illustrates a typical layout of the microfluidic manifold.

Following the study by Lim *et al.*,[6] all networks have been restricted to four generations (n = 0, 1, 2, 3). In the case of the square geometry, the dimension of the inlet channel (n = 0) was specified to be 250 μm, as used by Lim *et al.* Subsequent generations of the square sections were designed in accordance with eqn (3), using values of X of 0.75, 1.0 and 1.25. Moreover, the design also obeys the biomimetic principle that the length of each segment is proportional to its hydraulic diameter. In addition, the square manifold designed by Lim *et al.* has been modelled using their reported channel dimensions of 250, 200, 160 and 125 μm. This particular system represents an approximation of Murray's law using nominal channel dimensions rounded to the nearest 10 microns. However, the

Table 1 Channel dimensions of square-sectioned microfluidic manifolds employed in the numerical study. Following Lim *et al.*,[6] the inlet channel (n = 0) is taken to be 250 μm square. With the exception of the $X \approx 1$ case, the channel dimensions are obtained directly from eqn (3)

	Channel dimensions, d_n/μm			
Bifurcation level, n	X = 0.75	X = 1.0	X = 1.25	$X \approx 1$[a]
0	250.0	250.0	250.0	250.0
1	218.4	198.4	184.2	200.0
2	190.8	157.5	135.7	160.0
3	166.7	125.0	100.0	125.0

[a] Artificial vascular system fabricated by Lim *et al.*,[6] approximating X = 1.0.

Table 2 Channel dimensions of constant-depth rectangular- and trapezoidal-sectioned microfluidic manifolds employed in the numerical study. Following Lim *et al.*,[6] the channels are taken to be 125 μm deep. The channel dimensions are obtained numerically by solving either eqn (14) for α_{n} or eqn (16) for γ_n

	Channel dimensions				
	Rectangular w_n/μm				Trapezoidal a_n/μm
Bifurcation level, n	X = 0.75	X = 1.0	X = 1.25	X = 1.0	X = 1.0
0	250.0	250.0	250.0	625.0	1000.0
1	177.7	143.3	123.0	312.9	536.7
2	132.0	91.8	71.4	171.5	323.9
3	101.7	62.5	44.2	106.3	230.1

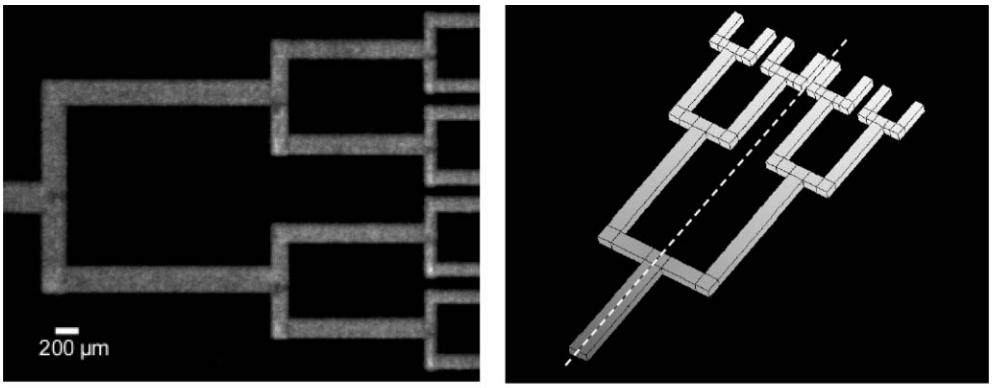

Fig. 3 Constant-depth rectangular manifold studied by Lim *et al.*[6] The system is composed of rectangular channels of widths 250, 200, 160 and 125 μm with a constant channel depth of 125 μm. (a) Image showing the artificial vascular system fabricated by Lim *et al.*[6] (reproduced by permission of the Royal Society of Chemistry). (b) Diagram showing the layout of the computational domain and the topological block structure used to perform the CFD simulations. The dashed line illustrates the plane of symmetry used to reduce the computational cost of the simulations.

segment lengths used by Lim *et al.* do not strictly adhere to the biomimetic principle of each segment length being proportional to its hydraulic diameter.

For the rectangular and trapezoidal cross-sections, the channel dimensions were obtained by solving either eqn (14) or (16), respectively. In all cases, the channel depth was 125 μm and the length of each segment followed the biomimetic principle of $L \propto D_h$. For the rectangular channel, the initial aspect ratio was taken to be 2 : 1 ($\alpha_0 = 0.5$) or 5 : 1 ($\alpha_0 = 0.2$), while the initial aspect ratio of the trapezoidal section was selected to be 8 : 1 ($\gamma_0 = 0.125$). In addition, the non-Murray law rectangular manifold fabricated by Lim *et al.*,[6] with channel widths of 250, 200, 160 and 125 μm, has also been modelled.

The numerical simulations were carried out using the commercial computational fluid dynamics software package, CFD-ACE+ (ESI CFD, Huntsville, USA).[22] The software uses a finite-volume algorithm to solve the non-linear Navier–Stokes equations governing the conservation of mass and momentum within the fluid. The meshes representing the vascular geometries contained approximately 1.0–2.4 million grid nodes depending upon the geometric cross-section and the value of X. The choice of grid resolution was based upon experience gained from previous validation studies on an extensive range of two- and three-dimensional laminar flows. Particular attention was paid to ensure that the simulations were fully converged (12 orders of magnitude reduction in the residuals). To reduce the computational cost of the simulations, a symmetry boundary condition was employed along the centreline of the inlet channel, as illustrated in Fig. 3b.

3.1 Numerical results

Definitive flow rates are not available from Lim *et al.*'s experimental study and therefore the present simulations have assumed a typical mean velocity of 0.01 ms^{-1} in all the inlet channels. The fluid within the manifold is assumed to be pure water with a dynamic viscosity of 0.001 kg m^{-1} s^{-1}. For the trapezoidal geometry, the Reynolds number in the inlet channel, $Re_0 = (\rho V_0 D_{h0})/\mu$, is 2.14 whereas for the square channel the Reynolds number will be 2.5.

Fig. 4 shows a comparison of the theoretical and predicted normalised wall shear stress distributions, $\bar{\tau}_n/\bar{\tau}_0$, where $\bar{\tau}_0$ is the mean shear stress in the inlet channel. For Murray's law ($X = 1$), the predicted shear stress distribution within the branching network remains identical in each successive generation. In contrast, changing the value of X allows the stress distribution in the manifold to be controlled. For example, using a value of $X = 0.75$ results in a shear stress distribution that continuously decreases as the flow progresses to the finer branches of the vascular network. Conversely, for $X = 1.25$, the shear stress will increase as the fluid travels

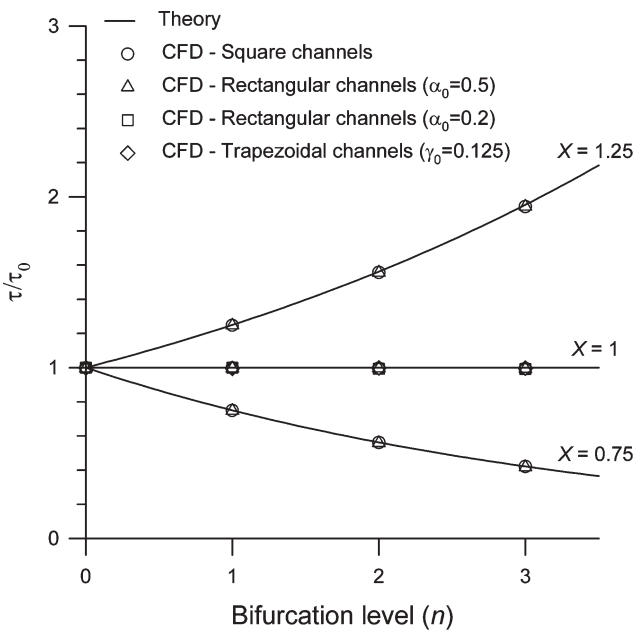

Fig. 4 Normalised shear stress distribution as a function of bifurcation level, n, in a series of microfluidic manifolds that obey the generalised form of Murray's law. Comparison of theoretical results from eqn (8) and CFD predictions (symbols).

through the hierarchical structure. Fig. 4 shows that the agreement between theory and simulation is excellent. There are also potential benefits to be gained by being able to predict and control the shear stress at each generation. For example, in cell response studies, a low shear stress environment will minimise damage to shear-sensitive cells[23] and will increase the probability of cells binding to surfaces.[24] Conversely, it may be desirable to increase the shear stress at each generation. For example, the transport of heavily-laden particulate flows may benefit from a controlled increase in shear stress to minimise blockage problems in the smaller channels.

A knowledge of the flow resistance and pressure distribution is also a key element in the design process. Fig. 5a shows how varying the branching parameter affects the flow resistance. When Murray's law is obeyed ($X = 1$), eqn (22) reduces to $R_T = (N + 1)R_0$ and the resistance of successive generations is identical. The total resistance to the flow therefore increases linearly with the number of generations. This is clearly demonstrated in Fig. 5a. For $X > 1$, the resistance of the structure increases with bifurcation level. Conversely, for $X < 1$, the resistance of subsequent generations decreases and the total resistance will tend to a constant value of $R_T = R_0/(1 - X)$ as $N \rightarrow \infty$. Again, the agreement between theory and simulation is very good.

Fig. 5b illustrates how the pressure distribution within the manifold is affected by the branching parameter. For $X < 1$, the most significant pressure loss occurs in the inlet channel ($n = 0$) with the pressure drop gradually diminishing at each successive generation, leading to a concave pressure distribution. Conversely, for $X > 1$, the pressure drop becomes more important towards the outlet of the artificial vascular system, leading to a convex pressure profile. When $X = 1$ (Murray's law), the pressure loss along each successive generation remains constant, leading to a linear pressure distribution within the microfluidic manifold. For all channel geometries, the CFD results agree very well with eqn (23).

The normalised shear stress, resistance and pressure distributions presented in Fig. 4 and 5 demonstrate that the flow characteristics are unaffected by the shape of the channels. The biomimetic principle proposed in eqn (8), based on Murray's law, leads directly to eqn (9) which is independent of the cross-sectional geometry. The design rule proposed in this paper is therefore applicable to all channels; the only practical limitation is the requirement to know the hydraulic diameter and the Poiseuille number of the desired channel.

Lim *et al.*[6] performed a flow visualisation study using fluorescent microbeads. They presented their data in the form of histograms showing the mean flow velocity as a function of bifurcation level in both square (multi-depth) and rectangular (uniform depth) microfluidic manifolds. Fig. 6 compares the theoretical predictions, CFD simulations, and experimental data. The large error bars associated with the experimental data indicate the difficulty in obtaining accurate measurements of the flow velocity. As previously stated, the design considered by Lim *et al.* does not strictly adhere to the biomimetic principle of $L \propto D_h$. Although this will not affect the mean velocity in each generation, it will influence the pressure distribution and flow resistance.

The theoretical description in Section 2 has assumed that the flow is laminar and fully-developed. However, the theory does not take account of the pressure losses associated with the T-junctions and 90° bends found in the example used. For low Reynolds number flows, these losses are negligible, as illustrated in Fig. 5a and b. Nevertheless, it is important to understand the limitations of the current theoretical description. Fig. 7 shows how the scaled flow resistance of a square

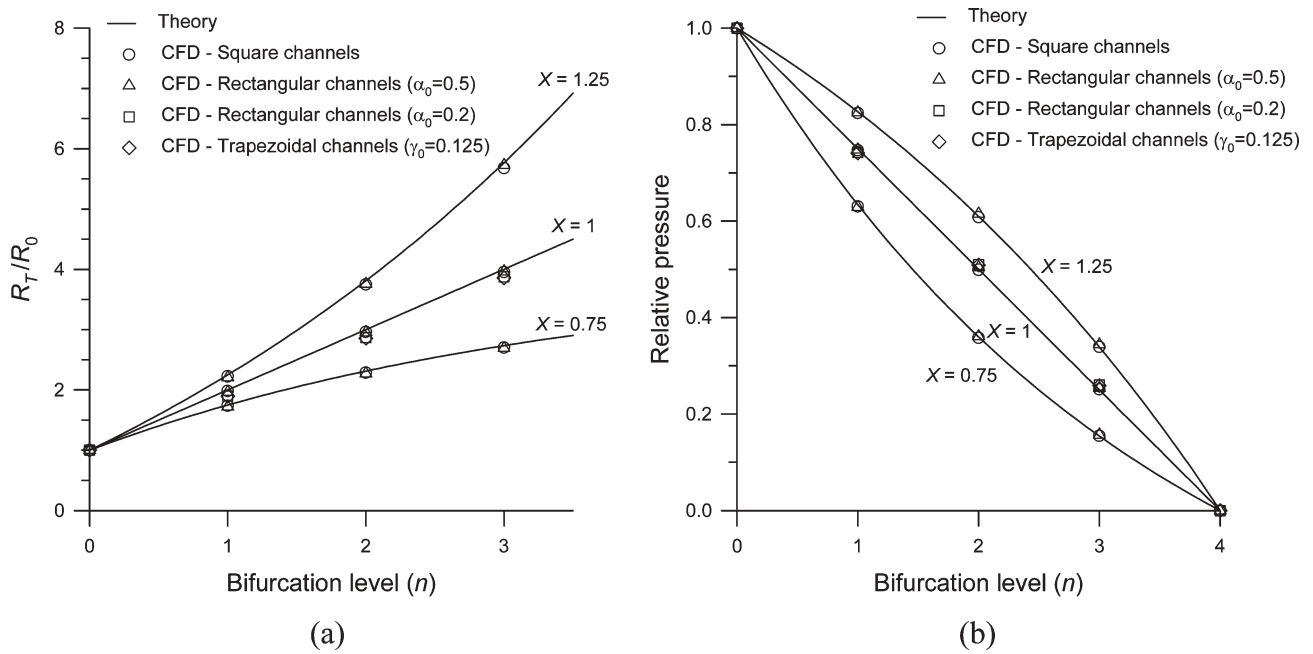

Fig. 5 Normalised flow resistance, R_T/R_0, and pressure distribution as a function of bifurcation level, n, in a series of microfluidic manifolds that obey the generalised form of Murray's law. Comparison of theoretical results (lines) and CFD predictions (symbols). The theoretical results for the flow resistance are computed using eqn (22) while the theoretical results for the normalised pressure distribution are obtained from eqn (23).

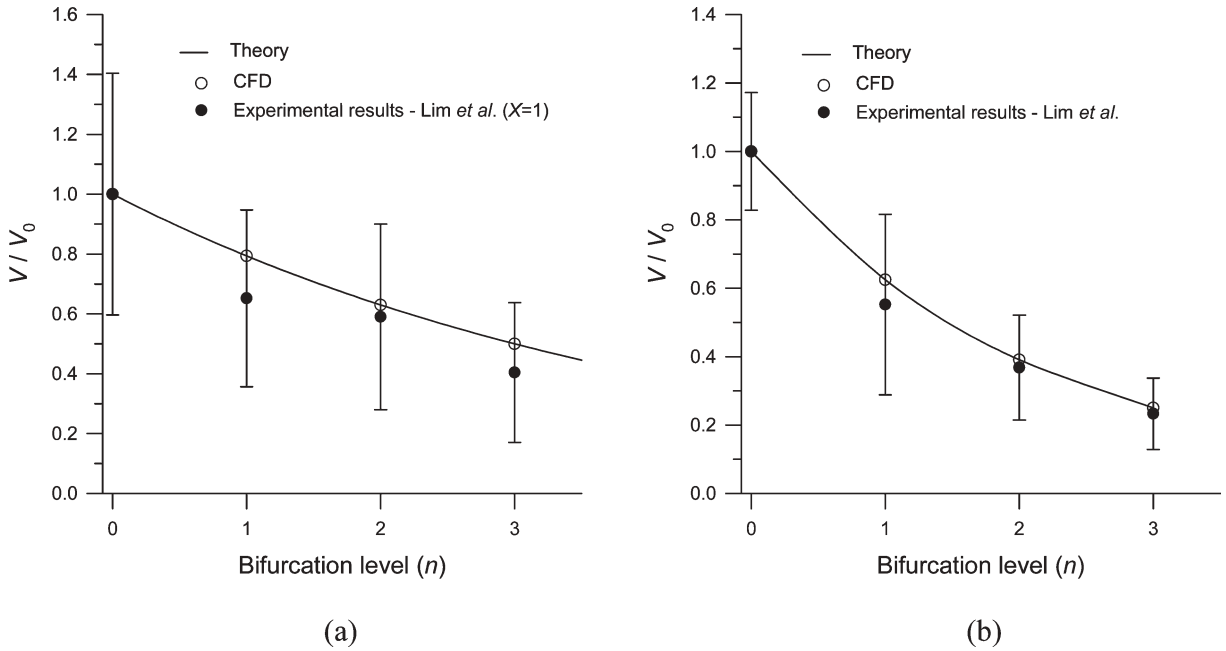

Fig. 6 Normalised mean flow velocity, V/V_0, as a function of bifurcation level, n, in the microfluidic manifolds studied by Lim *et al.*[6] Comparison of theoretical results (lines), CFD predictions (○) and Lim *et al.*'s experimental data (●). (a) Microfluidic manifold composed of multi-depth square channels of dimensions 250, 200, 160 and 125 μm that closely approximate Murray's law ($X = 1$). Theoretical results obtained from eqn (4). (b) Microfluidic manifold composed of rectangular channels (widths equal to 250, 200, 160 and 125 μm; uniform depth of 125 μm). Theoretical results computed using eqn (10).

manifold changes with inlet Reynolds number. For $Re_0 \leqslant 25$, the error in the predicted flow resistance is less than 2%. For $Re_0 = 50$, the theory underpredicts the CFD results by approximately 6% and this error grows to around 30% at $Re_0 = 250$. The pressure losses can be attributed to the formation of secondary eddies at each bend (see electronic supplementary information†). This effect will be felt most strongly within the initial stages of the manifold where the local Reynolds number is highest. Moreover, the secondary eddies create a localised flow constriction that increase frictional losses on the opposite wall. The Reynolds number limit could be increased by designing manifold layouts that incorporate features to reduce the observed frictional losses, such as Y-junctions or radial bends.

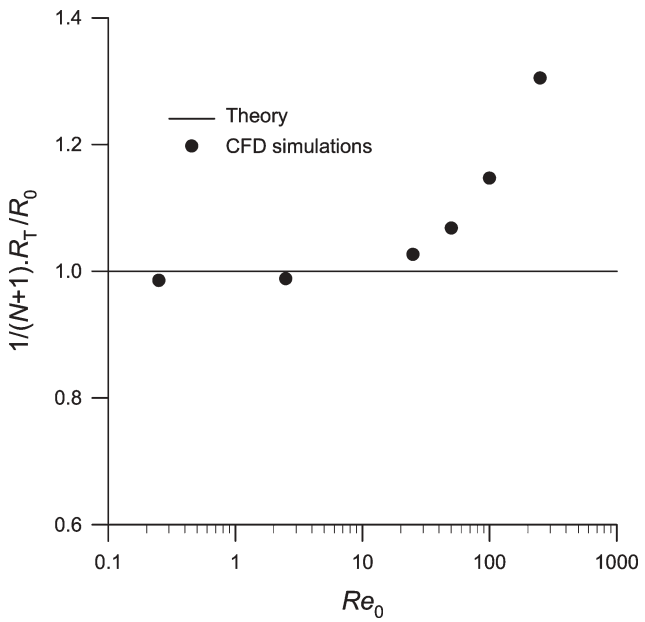

Fig. 7 Normalised flow resistance, $1/(N + 1) \times R_T/R_0$, as a function of inlet Reynolds number, Re_0, in a square microfluidic manifold obeying Murray's law ($X = 1$). Comparison between theory (line) and CFD predictions (●). For $Re_0 \leqslant 25$, the error in the theoretical flow resistance is less than 2% of that computed by CFD. However, this error grows with Reynolds number and at $Re_0 = 250$, the theory underpredicts the flow resistance by approximately 30%.

4 Concluding remarks and discussion

A generalised form of Murray's law has been developed that can be applied to the design of microfluidic channels and manifolds found in lab-on-a-chip systems. Murray's law was originally developed for cardiovascular systems composed of multi-diameter circular pipes and the present theory has used this biological principle to design constant-depth artificial vascular systems composed of rectangular or trapezoidal cross-sections. Biomimetic principles can now be applied to microfluidic devices fabricated using conventional batch processing techniques. This novel design approach removes the need to fabricate complex, multi-depth microstructures which would otherwise require difficult multi-exposure and alignment steps.

An assessment of the generalised form of Murray's law was carried out by performing a series of CFD simulations on branching fluidic manifolds composed of either square, rectangular or trapezoidal cross-sections. For the structures considered in the present study, the numerical simulations are

in very good agreement with the theoretical predictions of tangential shear stress, flow resistance, and pressure drop up to a Reynolds number of 30. Above this Reynolds number, the frictional losses associated with the sharp 90° bends will become increasingly significant.

Murray's law was originally derived from biological considerations and its applicability to microfluidic structures is only just being recognised. The present generalised theory has shown that by carefully selecting the branching parameter governing each bifurcation, it is possible to introduce a prescribed element of control into the flow behaviour. For example, hydrodynamic forces may damage shear-sensitive cells and the ability to predict and control a low-shear environment within the network could benefit cell response studies involving free-flowing or anchored cells. It is anticipated that the present design methodology could provide genuine benefits in the further development of lab-on-a-chip systems.

Acknowledgements

The authors would like to acknowledge partial support from the Framework VI PATENT DfMM Network of Excellence (contract no. 507255). Additional support was provided by the UK Engineering and Physical Sciences Research Council (EPSRC) under the auspices of Collaborative Computational Project 12 (CCP12).

References

1 M. Surge and S. N. Gorb, *J. Micromech. Microeng.*, 2000, **10**, 359–364.
2 J. Moorthy and D. J. Beebe, *Anal. Chem.*, 2003, **75**, 292A–301A.
3 J. Atencia and D. J. Beebe, *Lab Chip*, 2004, **4**, 598–602.
4 W. C. Chang, L. P. Lee and D. Liepmann, *Lab Chip*, 2005, **5**, 64–73.
5 F. G. Bessoth, A. J. deMello and A. Manz, *Anal. Commun.*, 1999, **36**, 231–215.
6 D. Lim, Y. Kamotani, B. Cho, J. Mazumder and S. Takayama, *Lab Chip*, 2003, **3**, 318–323.
7 C. D. Murray, *Proc. Natl. Acad. Sci. USA*, 1926, **12**, 207–214.
8 T. F. Sherman, *J. Gen. Physiol.*, 1981, **78**, 431–453.
9 M. Zamir, *J. Gen. Physiol.*, 1976, **67**, 213–222.
10 M. Zamir, *J. Gen. Physiol.*, 1977, **69**, 449–461.
11 Y. Zhou, G. S. Kassab and S. Molloi, *Phys. Med. Biol.*, 1999, **44**, 2929–2945.
12 A. Roth-Nebelsick, D. Uhl, V. Mosbrugger and H. Kerp, *Ann. Bot.*, 2001, **87**, 553–566.
13 K. A. McCulloh, J. S. Sperry and F. R. Adler, *Nature*, 2003, **421**, 939–942.
14 G. B. West, J. H. Brown and B. J. Enquist, *Science*, 1997, **276**, 122–126.
15 G. B. West, *Physica A*, 1999, **263**, 104–113.
16 K. Cieślicki, *Pol. J. Med. Phys. Eng.*, 1999, **5**, 161–172.
17 F. M. White, *Viscous Fluid Flow*, New York, McGraw-Hill, 2nd edn, 1991.
18 R. K. Shah and A. L. London, *Laminar Flow Forced Convection in Ducts*, New York, Academic Press, 1978.
19 W. H. Press, S. A. Teukolsky, W. T. Vetterling and B. P. Flannery, *Numerical Recipes in FORTRAN: The Art of Scientific Computing*, Cambridge Univ. Press, 2nd edn, 1992.
20 G. L. Morini, *J. Fluids Eng.*, 2004, **126**, 485–489.
21 B. J. West, *Fractal Physiology and Chaos in Medicine*, Singapore, World Scientific, 1990.
22 *CFD-ACE+ User Manual: Version 2004*, CFD Research Corporation, Huntsville, AL.
23 N. Ma, K. W. Koelling and J. J. Chalmers, *Biotechnol. Bioeng.*, 2002, **80**, 428–437.
24 J. G. Auniņš, B. Bader, A. Caola, J. Griffiths, M. Katz, P. Licari, K. Ram, C. S. Ranucci and W. Zhou, *Biotechnol. Prog.*, 2003, **19**, 2–8.

